Scientific Research Publishing

Open Journal of Applied Sciences, 2026, 16(6), 2039-2057
https://www.scirp.org/journal/ojapps
ISSN Online: 2165-3925
ISSN Print: 2165-3917

Urban Heat Island Effects during Heatwave Periods in Dalian from the Perspective of Local Climate Zones

Linze Li, Gaoyu Li

School of Geography, Liaoning Normal University, Dalian, China
Email: 15542689644@163.com

How to cite this paper: Li, L.Z. and Li, G.Y. (2026) Urban Heat Island Effects during Heatwave Periods in Dalian from the Perspective of Local Climate Zones. *Open Journal of Applied Sciences*, **16**, 2039-2057.
https://doi.org/10.4236/ojapps.2026.166113

Received: May 6, 2026
Accepted: June 2, 2026
Published: June 5, 2026

Abstract

Under the background of global climate warming and accelerated urbanization, the frequency and intensity of extreme heat events have continued to increase, leading to increasingly prominent urban thermal environmental issues in traditionally cold-region cities. During the summer of 2018, Northeast China experienced one of the most severe regional heatwave events in recent years. As a representative coastal cold-region city in China, Dalian exhibited a markedly intensified urban heat island effect under the influence of this extreme climatic event. This study focused on the main urban area of Dalian and used the Local Climate Zone (LCZ) classification framework in conjunction with remote sensing land surface temperature (LST) data to quantitatively analyze the spatial distribution characteristics of surface urban heat island intensity (SUHII) during the representative heatwave summer of 2018. Furthermore, multiple urban environmental factors were incorporated, and the GeoDetector model was used to systematically investigate the driving mechanisms underlying the urban heat island effect. The results indicate that: 1) the spatial distribution of LCZs in the main urban area of Dalian exhibited a distinct pattern characterized by "coastal agglomeration and inland transition", with different underlying surface types providing the fundamental basis for thermal environmental differentiation; 2) under heatwave conditions, the land surface thermal environment demonstrated significant spatial heterogeneity, with high-temperature areas primarily concentrated in the urban core and coastal industrial zones, whereas low-temperature areas were mainly regulated by water bodies and mountainous vegetation. Overall, the spatial pattern was characterized by "enhanced warming in built-up areas and localized cooling in ecological spaces", and the spatial distribution of SUHII corresponds well with LCZ types; 3) GeoDetector analysis revealed that surface imperviousness was the dominant driving factor, while water bodies and vegetation exert im-

portant regulatory effects. Population density also significantly influenced the spatial differentiation of the urban heat island effect, whereas topographic effects were comparatively limited; interactions among multiple factors all exhibited enhancement effects, among which the coupling of surface imperviousness with water bodies, vegetation, and human activities provided the strongest explanatory power for the spatial pattern of the urban heat island, indicating that the heat island effect was jointly driven by multiple factors and was substantially intensified through their combined interactions. The findings of this study can provide a scientific basis for thermal environment regulation and climate-adaptive urban planning in cold-region cities.

Keywords

Local Climate Zone (LCZ), Surface Urban Heat Island Intensity (SUHII), Heatwave, Cold-Region City, GeoDetector

1. Introduction

With the continuous concentration of urban populations and the increasing intensity of urban construction, natural land surfaces originally dominated by vegetation and soil have gradually been replaced by impervious materials such as concrete and asphalt. This transformation significantly alters the surface energy balance process, thereby leading to abnormal temperature increases in urban areas, commonly referred to as the Urban Heat Island (UHI) effect [1]. The urban heat island effect not only modifies the local urban climate environment, but also exacerbates energy consumption, air pollution, and public health risks, thereby posing serious challenges to sustainable urban development. Particularly under the increasingly frequent occurrence of heatwave events, the combined effects of UHI and extreme heat tend to amplify thermal environmental risks, resulting in higher incidences of heat-related illnesses and mortality [2]-[4]. Therefore, systematically investigating the spatial differentiation characteristics and formation mechanisms of the urban heat island effect under heatwave conditions is of considerable theoretical and practical significance for enhancing urban climate resilience and developing scientifically grounded thermal mitigation strategies.

From the perspective of research classification, the urban heat island effect is generally categorized into Atmospheric Urban Heat Island (AUHI) and Surface Urban Heat Island (SUHI) [5]. AUHI primarily relies on meteorological station observations and characterizes heat island intensity through air temperature differences between urban and suburban areas. This approach offers advantages such as long-term temporal records and high observational accuracy [6]; however, due to the sparse spatial distribution of monitoring stations, it is often unable to capture the fine-scale spatial heterogeneity within urban environments [7]. With the advancement of remote sensing technology, SUHI studies based on Land Surface Temperature (LST) have gradually become the mainstream approach, as they can

reveal thermal environmental differences among various urban functional zones at relatively high spatial resolutions and provide important support for analyzing the spatial patterns of urban heat islands [8]. In quantitative SUHI research, the calculation of Surface Urban Heat Island Intensity (SUHII) represents a central issue [9]. Traditional studies commonly use an urban-rural dichotomy, using the LST difference between urban and suburban areas as an indicator of SUHII. Although this method is simple and intuitive, it suffers from several limitations, including the subjective delineation of suburban boundaries, neglect of intra-urban surface heterogeneity, and limited adaptability to dynamic urban expansion [10]-[12]. To overcome these limitations, the Local Climate Zone (LCZ) framework was proposed [13]. This approach classifies urban areas into spatial units with similar thermal characteristics based on surface cover, urban structure, and human activity. By comparing different LCZ types, the method enables a more refined quantification of SUHII, thereby improving the comparability and scientific robustness of results while also providing a new framework for exploring the relationship between urban spatial morphology and heat island effects [14].

The formation of the urban heat island effect is jointly influenced by multiple factors, which can generally be categorized into natural environmental factors and human factors. Among the natural factors, topographic conditions play an important role in heat accumulation and dissipation processes by influencing solar radiation reception and air circulation, and are commonly characterized using a Digital Elevation Model (DEM) [15]. Vegetation cover can reduce land surface temperature through shading and evapotranspiration effects, and the Normalized Difference Vegetation Index (NDVI) is widely used to characterize its spatial distribution [16] [17]. Water bodies, as important "cooling sources", can effectively mitigate the urban heat island effect through evaporation. Previous studies have commonly used the Normalized Difference Water Index (NDWI) to characterize water distribution; however, because NDWI is sensitive to building shadows and soil background noise, the Modified Normalized Difference Water Index (MNDWI) has demonstrated higher identification accuracy in urban environments [15]. Regarding human factors, impervious surfaces are considered one of the key drivers intensifying the urban heat island effect. Earlier studies frequently used the Normalized Difference Built-up Index (NDBI) or Normalized Difference Soil Index (NDSI) to characterize surface imperviousness, whereas the Normalized Difference Built-up and Soil Index (NDBSI), by integrating multi-source information, can more comprehensively reflect urban impervious surface characteristics [18]. In addition, Population (POP) also exerts a significant influence on the urban heat island effect by affecting energy consumption and human heat emissions [19]. Methodologically, previous studies have primarily used correlation analysis and linear regression models to investigate the relationships between influencing factors and the urban heat island effect [20]-[23]. Although these methods are effective in revealing overall trends, they are generally based on assumptions of linear

relationships among variables, making it difficult to capture complex nonlinear interaction mechanisms. Moreover, they often overlook spatial heterogeneity, namely the substantial regional differences in the influence intensity of various factors on the urban heat island effect [24] [25]. To address these limitations, the GeoDetector method has gradually been introduced into urban thermal environment research [26]. Based on the principle of spatial stratified heterogeneity, this method can quantitatively evaluate the explanatory power of different factors on the spatial differentiation of the urban heat island effect and further reveal the interaction types among multiple factors. Consequently, it provides an effective tool for analyzing multi-factor coupling mechanisms and demonstrates broad application potential in studies of urban heat island driving mechanisms.

As a typical coastal cold-region city in China, Dalian is characterized by both maritime and temperate monsoon climatic features, with cold and windy winters, hot and humid summers. Its urban thermal environment evolution therefore exhibits strong regional representativeness. In recent years, with the continuous advancement of urbanization, the scale of construction land in Dalian's main urban area has expanded rapidly, accompanied by increasing concentrations of population and industrial activities and a substantial growth in impervious surfaces. Consequently, the urban spatial structure has gradually evolved from a traditional monocentric pattern toward a more polycentric and complex configuration. Meanwhile, human activities such as coastal development, transportation infrastructure construction, and the expansion of high-density residential areas have further altered the characteristics of the urban underlying surface, thereby intensifying the spatial heterogeneity of the urban thermal environment. Under the background of global climate warming, the frequency and intensity of extreme heat events have continued to increase, making urban heat island issues increasingly prominent even in cold-region and coastal cities. During the summer of 2018, Northeast China experienced one of the most severe regional heatwave events in recent decades. According to meteorological observations released by the China Meteorological Administration, multiple cities in Liaoning Province recorded persistent high-temperature conditions exceeding the historical climatological average. Dalian experienced continuous extreme high-temperature weather during late June and early August, with daily maximum temperatures exceeding 35˚C for several consecutive days, satisfying the official heatwave criterion of the China Meteorological Administration. Under the combined influence of extreme high temperatures and densely built-up urban surfaces, local heat accumulation was substantially intensified, further aggravating urban thermal environmental problems.

Based on this context, this study selected the main urban area of Dalian as the research area. First, the LCZ for 2018 was generated. Subsequently, summer LST data for 2018 were acquired and averaged using the Google Earth Engine (GEE) platform, and the SUHII was quantitatively characterized within the LCZ framework. On this basis, key urban environmental factors, including NDVI, MNDWI,

POP, NDBSI, and DEM, were selected. The GeoDetector method was then used to systematically analyze both the individual effects of these factors on SUHII and their pairwise interaction mechanisms. The study aims to reveal the formation mechanisms and driving factors of the urban heat island effect in coastal cold-region cities under heatwave conditions, thereby providing a scientific basis for thermal environment optimization and climate-adaptive regulation in Dalian and other cities with similar climatic characteristics.

2. Data and Methods

2.1. Study Area

Dalian is located at the southern tip of the Liaodong Peninsula in Northeast China, bordering both the Yellow Sea and the Bohai Sea (Figure 1). As a typical coastal cold-region city, it is jointly influenced by land-sea interactions and a temperate monsoon climate. The study area covers the main urban region of Dalian, where the overall terrain is characterized by higher elevations in the north and lower elevations in the south. The landforms are primarily composed of hills and terraces, resulting in complex underlying surface types and strong spatial heterogeneity. Influenced by the coastal topography, the local climate exhibits a certain degree of regulatory capacity; however, heat dissipation within densely built-up areas remains relatively limited, making these areas prone to heat accumulation. In terms of land cover patterns, the study area is dominated by urban

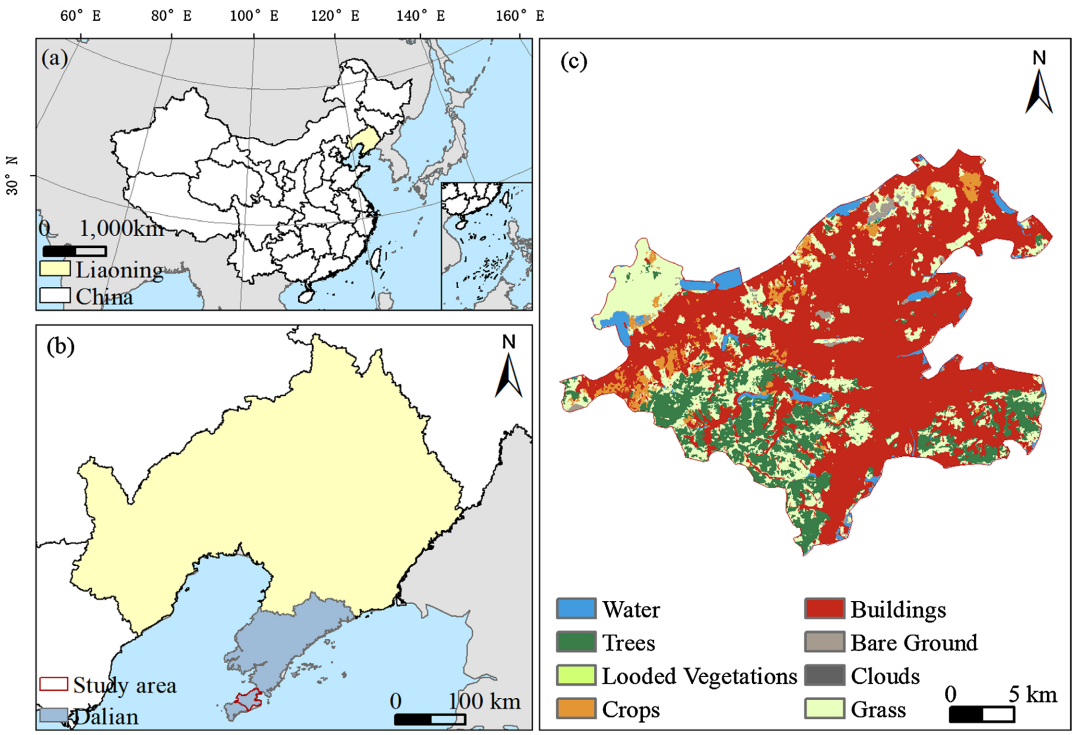

Source: http://bzdt.ch.mnr.gov.cn.

Figure 1. Location of the study area (a) Geographic location of Liaoning Province; (b) Geographic location of the study area; (c) Land cover types of the study area in 2018.

built-up land, with high-density building clusters distributed continuously, forming typical impervious surface concentration zones. Forests and grasslands are mainly distributed in the southern and peripheral hilly areas, while croplands are sparsely scattered along the urban fringe. Water bodies are distributed in linear or patchy forms along coastlines, reservoirs, and local rivers, exerting a certain cooling effect on the local thermal environment. Overall, the study area exhibits prominent built-up area agglomeration, uneven distribution of ecological spaces, and highly complex underlying surface structures. In recent years, rapid urbanization has driven the continuous expansion of construction land in Dalian's main urban area, leading to a persistent increase in impervious surface coverage and compression of ecological cooling spaces, thereby intensifying urban thermal environmental problems. Particularly during the heatwave event in the summer of 2018, the combined effects of extreme high temperatures and high-intensity built environments further enhanced surface heat accumulation, making the urban heat island effect and the spatial heterogeneity of the thermal environment more pronounced.

2.2. Data Sources and Preprocessing

2.2.1. Local Climate Zone (LCZ) Dataset

The LCZ data used in this study were obtained from the global 100 m resolution LCZ dataset provided by Demuzere *et al.* [27]. This dataset was developed based on a unified classification scheme and an automated mapping procedure, producing a globally consistent LCZ product that provides a standardized land surface classification framework for urban climate studies.

The LCZ dataset classifies the land surface into 17 representative types based on surface cover, structural characteristics, and human activity intensity (**Table 1**). Among them, LCZ1-LCZ10 represent built-up types, reflecting variations in building density and height, while LCZA-LCZG represent natural land cover

Table 1. Local climate zone (LCZ) classification and descriptions.

Land cover type	LCZ	Description	Land cover type	LCZ	Description
Built-up	LCZ 1	Compact high-rise	Built-up	LCZ 10	Heavy industry
	LCZ 2	Compact mid-rise			
	LCZ 3	Compact low-rise	Natural	LCZ A	Dense trees
	LCZ 4	Open high-rise		LCZ B	Scattered trees
	LCZ 5	Open mid-rise		LCZ C	Shrubland
	LCZ 6	Open low-rise		LCZ D	Grassland
	LCZ 7	Lightweight low-rise		LCZ E	Paved surfaces
	LCZ 8	Large low-rise buildings		LCZ F	Bare soil
	LCZ 9	Sparsely built		LCZ G	Water bodies

types, including vegetation, water bodies, and bare soil. This classification system effectively captures urban morphological characteristics and associated thermal properties, and has become a widely used foundational dataset in urban thermal environment research.

During data preprocessing, the global LCZ dataset covering the study area was first acquired and then spatially clipped using the vector boundary of the main urban area of Dalian to extract LCZ information within the study extent. The clipped LCZ dataset was used as the fundamental dataset for subsequent analyses, serving to characterize different underlying surface types and to support the calculation of SUHII as well as the analysis of its driving mechanisms.

2.2.2. Land Surface Temperature and Urban Environmental Datasets

The LST and various urban environmental datasets used in this study are summarized in Table 2. All environmental predictor datasets used in this study represent conditions for the year 2018 to ensure temporal consistency with the analyzed heatwave event. NDVI, MNDWI, and NDBSI were derived from Landsat 8 imagery acquired during the same heatwave period as the LST dataset. The POP dataset corresponds to the 2018 population distribution product obtained from the WorldPop database, while the DEM dataset represents stable topographic conditions and therefore required no temporal adjustment. These datasets characterize the thermal environment of the study area and its potential driving factors from multiple perspectives, including vegetation coverage, water distribution, human activity intensity, surface imperviousness, and topographic conditions.

Given the inconsistencies in spatial resolution and coordinate reference systems among different data sources, all datasets were first projected into a unified coordinate reference system and spatially harmonized. NDVI, MNDWI, and NDBSI were calculated on the GEE platform using standard spectral index formulas based on atmospherically corrected Landsat 8 imagery. The POP dataset was resampled from its original spatial resolution to 100 m using bilinear interpolation, while the DEM dataset was resampled using nearest-neighbor interpolation to preserve terrain characteristics. This process ensured a consistent dataset for subsequent SUHII calculation and GeoDetector analysis.

Table 2. Data sources.

Data type	Resolution	Data sources	Representation type
LST	30 m	https://code.earthengine.google.com/	Thermal environment
NDVI	30 m	https://code.earthengine.google.com/	Vegetation
MNDWI	30 m	https://code.earthengine.google.com/	Water bodies
POP	100 m	https://zenodo.org/records/8214467	Human activity
NDBSI	30 m	https://code.earthengine.google.com/	Surface imperviousness
DEM	90 m	https://www.gscloud.cn/search	Topography

2.3. Methods

2.3.1. Land Surface Temperature Retrieval and Urban Heat Island Intensity Calculation

In this study, Land Surface Temperature (LST) retrieval for the study area was conducted using the GEE platform. To ensure consistency with the heatwave-oriented objective of this study, Landsat 8 scenes acquired during the heatwave period from 18 June to 15 August 2018 were initially collected. During the data processing stage, cloud and cloud-shadow contamination was removed using cloud masking methods provided by the Google Earth Engine platform. A multi-temporal median compositing method was applied to generate the final LST dataset for the heatwave period, which effectively reduced residual cloud contamination and random noise. For pixels remaining missing after compositing, a neighborhood-based focal interpolation method was used to restore spatial continuity and improve dataset completeness.

In this study, SUHII was calculated following the approach proposed by Bechtel *et al.* [28], and the formula is given as follows:

$$SUHII_x = LST_x - LST_{LCZ(A\text{-}D)} \quad (1)$$

where: $SUHII_x$ represents the heat island intensity of pixel x, LST_x denotes the land surface temperature of pixel x; and $LST_{LCZ(A\text{-}D)}$ represents the mean LST of LCZ A, B, C, and D. In this study, LCZ A-D were selected as the reference background because these LCZ types mainly represent natural vegetation-covered surfaces with relatively low human disturbance and stable thermal characteristics, which can effectively reduce uncertainties associated with traditional urban-rural dichotomy approaches and improve inter-city comparability of SUHII estimation [29].

In this study, SUHII was classified into three major categories: cold island, neutral, and heat island zones, and further subdivided into five levels, namely strong cold island, moderate cold island, normal temperature zone, moderate heat island, and strong heat island. Among them, cold and heat island zones represent areas with pronounced cooling and warming effects, respectively, while the normal temperature zone indicates relatively stable thermal conditions. The specific classification thresholds are presented in **Table 3**:

Table 3. Urban heat island classification scheme.

Zone type	Heat island category	SUHII range (˚C)
Cold island	Strong cold island	SUHII≤ −3
	Moderate cold island	−3 < SUHII ≤ −1
Neutral zone	Normal temperature zone	−1 < SUHII ≤ 1
Heat island	Moderate cold island	1 < SUHII ≤ 3
	Strong heat island	3 < SUHII

2.3.2. GeoDetector Analysis

In this study, the factor detector and interaction detector modules of the GeoDe-

tector model were used to quantitatively analyze the driving mechanisms of the spatial differentiation of the surface thermal environment in the main urban area of Dalian under heatwave conditions. SUHII was used as the dependent variable (Y), while a set of natural and anthropogenic factors—including vegetation coverage, water conditions, surface imperviousness, population activity intensity, and topographic conditions—were selected as independent variables (X_i).

Prior to model implementation, all driving factors were discretized using the natural breaks classification method. Each variable was divided into five classes to ensure comparability among different factors while preserving spatial heterogeneity characteristics. The spatial analysis unit of the GeoDetector model was based on 100 m raster grid cells corresponding to the unified spatial resolution of the datasets.

The factor detector was used to quantify the explanatory power of each individual driving factor on the spatial variation of SUHII. Its core metric is the q-statistic, which measures the extent to which an independent variable X_i explains the spatial heterogeneity of the dependent variable Y. A higher q value indicates a stronger explanatory power of the factor on the spatial pattern of the urban heat island, thereby enabling the identification of dominant driving factors and their relative contributions. Statistical significance tests for the q-statistics were conducted using permutation testing within the GeoDetector framework, and all reported p-values were significant at the 0.001 level. The specific formula is given as follows:

$$q\left(X_i\right)=\frac{\sum_{h=1}^{L} N_h \sigma_h^2}{N\sigma^2},\ q\left(X_i\right)\in\left[0,1\right] \tag{2}$$

where $h=1,\cdots,L$ denotes the stratification of Y or X_i; N_h and N represent the number of units in layer h and the entire study area, respectively; and σ_h^2 and σ^2 denote the variance of Y within layer h and the variance of Y across the whole study area, respectively. A larger $q(X_i)$ value indicates a stronger influence of the corresponding driving factor on the spatial heterogeneity of SUHII.

On this basis, the interaction detector was further used to examine the coupling effects between any two driving factors (Table 4). By spatially overlaying two

Table 4. Types of interaction effects between X_i and X_j on SUHII Interaction type.

Interaction type	Criterion
Nonlinear weakening	$q\left(X_i\cap X_j\right)<\min\left[q\left(X_i\right),q\left(X_j\right)\right]$
Univariate nonlinear weakening	$\min\left[q\left(X_i\right),q\left(X_j\right)\right]<q\left(X_i\cap X_j\right)<\max\left[q\left(X_i\right),q\left(X_j\right)\right]$
Bivariate enhancement	$q\left(X_i\cap X_j\right)>\max\left[q\left(X_i\right),q\left(X_j\right)\right]$
Independence	$q\left(X_i\cap X_j\right)=q\left(X_i\right)+q\left(X_j\right)$
Nonlinear enhancement	$q\left(X_i\cap X_j\right)>q\left(X_i\right)+q\left(X_j\right)$

factors to generate a new composite stratification variable, the combined explanatory power on SUHII, $q\left(X_i \cap X_j\right)$, is calculated. This allows for comparison between the explanatory power of individual factors and that under interaction, thereby revealing how factor interactions enhance or weaken their influence on SUHII.

3. Results

3.1. Local Climate Zones in Dalian

From an overall spatial perspective, the LCZs in the main urban area of Dalian exhibited a distinct pattern characterized by "coastal agglomeration and inland transition" (Figure 2). Built-up LCZs (LCZ1-10) were primarily concentrated in the urban core and coastal areas, forming a continuous and highly clustered spatial pattern. In contrast, natural LCZs (LCZA-G) were mainly distributed in the peripheral and southern hilly regions, generally appearing in patchy or linear forms. Influenced jointly by mountainous and coastal topography, the LCZ distribution showed pronounced spatial heterogeneity, reflecting the coexistence of urban expansion and ecological space compression.

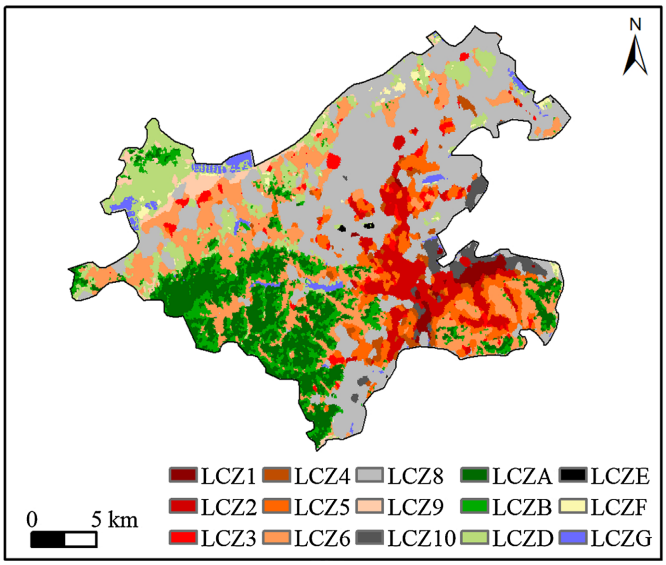

Figure 2. Local Climate Zone (LCZ) map of the main urban area of Dalian.

Within built-up LCZs, LCZ2 (compact mid-rise), LCZ3 (compact low-rise), and LCZ5 (open mid-rise) were the dominant types. These were widely distributed in the urban core and represented the most concentrated built-up areas. Specifically, LCZ2 and LCZ3 exhibited contiguous and highly aggregated patterns with relatively high building density, indicating areas with strong heat accumulation potential. LCZ5 is mainly located in peripheral residential zones and newly developed districts, reflecting a relatively open urban form. LCZ8 (large low-rise buildings) was scattered across industrial zones, ports, and logistics areas, highlighting the characteristics of a coastal industrial and port city. In comparison,

LCZ1 (compact high-rise) and LCZ4 (open high-rise) occupied smaller areas and were mainly found in localized high-density commercial districts and newly developed urban zones.

Among natural LCZs, LCZA (dense trees) and LCZB (scattered trees) were mainly concentrated in the southern and southwestern hilly regions, forming relatively large and continuous ecological patches. LCZD (low vegetation) was widely distributed in urban-rural transition zones and some urban fringes. LCZG (water bodies) appeared in linear or patchy forms along coastlines, reservoirs, and local rivers, playing an important role in regulating the regional thermal environment. LCZE (bare or impervious ground) was sparsely distributed and generally occurs in isolated patches. Overall, natural LCZs showed limited spatial continuity and relatively fragmented distribution patterns.

In general, the LCZ pattern of Dalian's main urban area was characterized by "coastal concentration of built-up areas and peripheral distribution of ecological spaces". Significant spatial heterogeneity existed among different LCZ types, providing an important underlying surface basis for subsequent analyses of land surface temperature distribution and urban heat island effects. This spatial pattern also reflected typical characteristics of thermal environment evolution in coastal cold-region cities under urban expansion.

3.2. Characteristics of the Urban Heat Island Effect under Heatwave Conditions in Dalian

From an overall spatial distribution perspective, the LST of the main urban area of Dalian in the summer of 2018 exhibited pronounced spatial heterogeneity, characterized by a pattern of "high-temperature clustering in built-up areas and low-temperature distribution in ecological spaces" (Figure 3). High-temperature zones were primarily concentrated in the central-eastern urban core and coastal

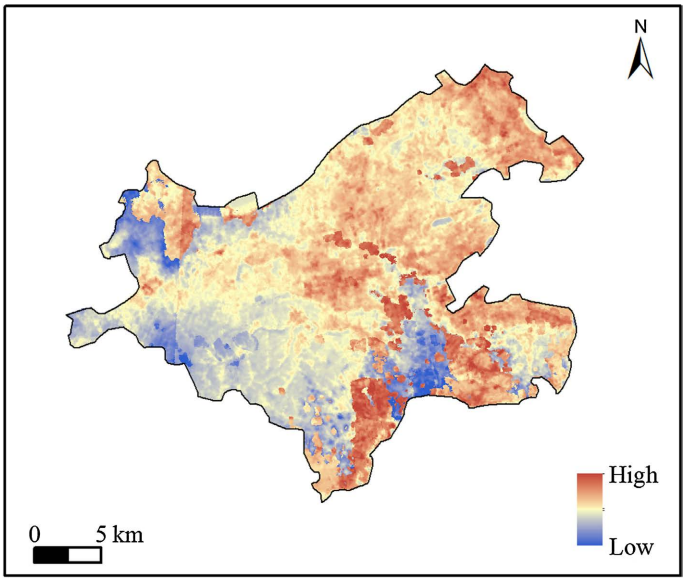

Figure 3. Summer Land Surface Temperature (LST) map of the main urban area of Dalian.

built-up areas, forming relatively continuous hot patches. In contrast, low-temperature areas were mainly located in the western and southern hilly regions with dense vegetation cover, as well as around local water bodies, generally appearing in patchy or linear forms and providing a certain cooling effect on the regional thermal environment.

In terms of detailed spatial characteristics, high-temperature areas showed strong spatial consistency with high-density built-up regions. Areas with dense construction and a high proportion of impervious surfaces were more prone to heat accumulation. In addition, coastal industrial and port zones also exhibited relatively high land surface temperatures, indicating the significant influence of human activities on the thermal environment. By contrast, mountainous and hilly areas with higher vegetation coverage, as well as regions surrounding water bodies, generally presented lower surface temperatures, suggesting that vegetation transpiration and water evaporation played an effective role in mitigating local thermal conditions. Furthermore, a number of scattered low- and medium-temperature patches were observed within the study area, indicating that the urban thermal environment exhibited notable fine-scale spatial variability, closely associated with complex underlying surface conditions.

The average land surface temperature in the study area during the summer of 2018 was 32.41˚C, indicating an overall high thermal level. This suggests a significantly intensified urban thermal load under heatwave conditions. The superposition of extreme high temperatures and high-density built environments further exacerbated local heat accumulation, leading to more pronounced spatial differentiation of the urban thermal environment within the city.

Based on the LCZ and land surface temperature data, this study derived the summer SUHII for the main urban area of Dalian in 2018, together with its spatial pattern and the proportion of heat island types across different LCZ classes (**Figure 4**). The urban heat island exhibited a clear spatial differentiation pattern

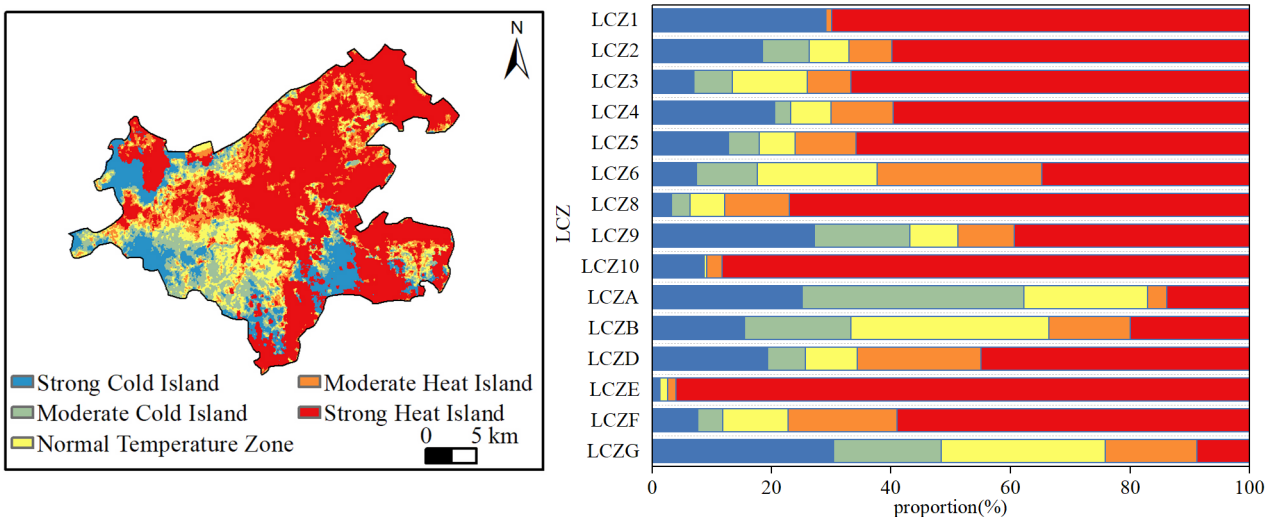

Figure 4. Summer SUHII and proportions of heat island types across Local Climate Zones in the main urban area of Dalian.

characterized by strong heat island clustering in the central urban core and an interwoven distribution of cold sources in suburban, coastal, and mountainous ecological areas. This pattern was highly consistent with both the LCZ-based underlying surface structure and the spatial distribution of LST. Strong heat island zones were mainly concentrated in the core built-up districts of Zhongshan, Xigang, Shahekou, and Ganjingzi, forming contiguous urban clusters. Cold and strong cold island areas were distributed in a patchy and linear mosaic pattern along the eastern coastal belt, southern mountainous forests, and western ecological corridors. Normal temperature zones were primarily located in urban–rural transition areas, peripheral built-up regions, and port-adjacent zones, functioning as thermal buffer areas.

Different LCZ types exhibited pronounced differences in thermal responses, confirming the applicability of the LCZ framework in fine-scale urban thermal environment analysis. Built-up LCZs were the primary contributors to urban heat island formation. Compact high-rise areas and industrial land exhibited the highest proportion of strong heat island conditions, followed by compact low-rise and large low-rise building zones. Open mid-rise areas showed a moderate proportion of heat island conditions, while open low-rise and sparsely built areas were dominated by normal temperature zones and cold island components, reflecting the regulatory effects of building density and spatial openness on local thermal conditions.

Natural and ecological LCZs demonstrate distinct cooling source differentiation. Water bodies (LCZG) exhibited the most significant cooling effect, with a dominant proportion of cold island conditions. Dense forest areas also provide strong cooling potential, with relatively high proportions of cold and normal temperature zones. In contrast, sparse trees and grassland/cropland areas were mainly characterized by normal temperature zones, with mixed thermal properties and weaker cooling capacity compared to water bodies and dense forests, indicating the limiting role of vegetation coverage in cooling efficiency. Artificial surfaces and bare soil areas exhibit thermal characteristics similar to built-up land, with a relatively high proportion of strong heat island conditions, further exacerbating regional thermal stress.

In summary, the spatial differentiation of the urban heat island in the main urban area of Dalian was primarily controlled by differences in the thermal properties of LCZ-based underlying surfaces. Built-up land served as the dominant heat source, while water bodies and dense forests acted as the primary cooling sources. The spatial configuration of these elements jointly shapes the urban heat island pattern. These findings provide scientific support for thermal environment optimization, ecological planning, and adaptive urban management in coastal cities under heatwave conditions.

3.3. Influence of Urban Environmental Factors on the Urban Heat Island Effect under Heatwave Conditions in Dalian

This study selected five key influencing factors, including NDVI, MNDWI, POP,

NDBSI, and DEM. Their spatial distributions are shown in Figure 5.

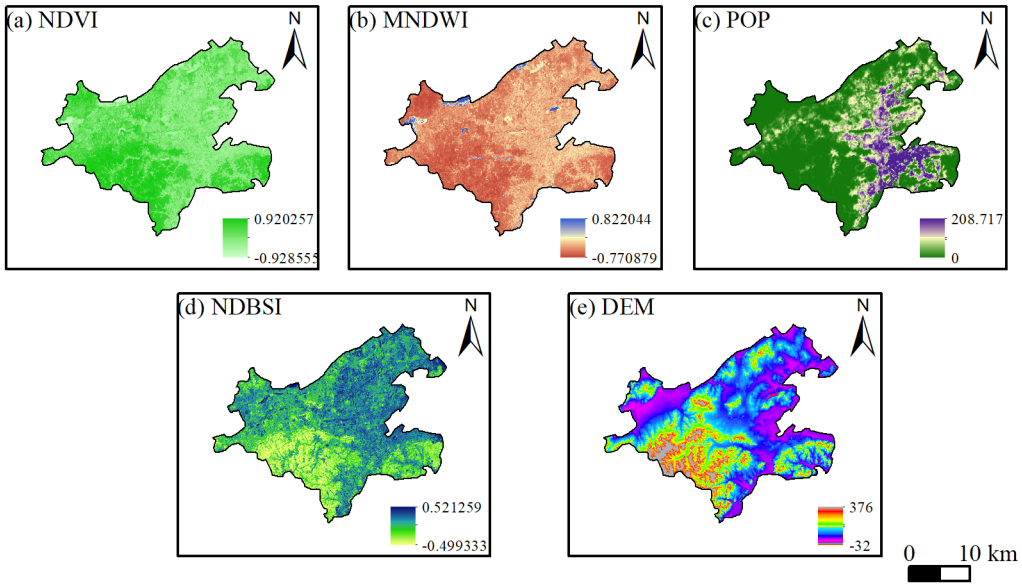

Figure 5. Spatial distribution characteristics of key driving factors of the urban heat island effect.

NDVI generally exhibited a pattern characterized by "high values across the region with localized low-value clusters." High NDVI values were widely distributed in peripheral mountainous forests and ecological green spaces, while contiguous low-value areas were observed in the central urban built-up zones, clearly reflecting the spatial heterogeneity of vegetation coverage. NDBSI high-value areas were concentrated in the urban core and coastal industrial zones, showing a strong spatial coupling with impervious surfaces and directly indicating the degree of surface imperviousness. MNDWI high values were distributed in linear and patchy forms along coastal waters and inland river systems, accurately representing the spatial pattern of water bodies in the study area.

Population density (POP) presented a "core aggregation with a decreasing gradient outward" pattern, with significantly higher values in the urban center, which strongly overlapped with areas of intense heat island effects. The DEM indicated an overall topographic gradient declining from northwest to southeast, with terrain undulations mainly concentrated in the southern and eastern hilly regions, while the central urban area remained relatively flat.

Overall, these variables comprehensively characterize the urban environmental conditions influencing the heat island effect in the main urban area of Dalian from five dimensions: vegetation, water bodies, anthropogenic activity, surface imperviousness, and topography.

The factor detector results based on the GeoDetector model (Figure 6) indicated that the explanatory power of different driving factors for the spatial heterogeneity of SUHII in the main urban area of Dalian exhibited a clear hierarchical pattern. The ranking of q values was as follows: NDBSI > MNDWI > NDVI > POP > DEM (all p-values < 0.001, indicating statistical significance). Among these

factors, NDBSI exhibited the highest q value and thus served as the dominant driver of the spatial pattern of the urban heat island. This highlights the strong influence of impervious surfaces and hardened underlying surfaces in shaping the urban thermal environment. MNDWI and NDVI showed moderate explanatory power, reflecting the cooling effects of coastal water bodies and vegetation cover, respectively, both of which acted as key regulators of the regional thermal environment. POP ranked next, indicating that population concentration and anthropogenic activity intensity have a substantial impact on the urban heat island effect. DEM showed the lowest explanatory power, suggesting that topographic conditions play a relatively limited direct role in shaping the spatial variability of the thermal environment in the study area.

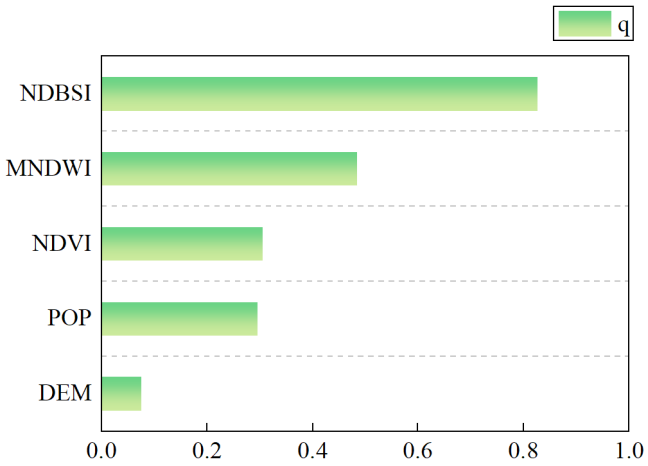

Figure 6. Results of the GeoDetector-based analysis of driving factors of the urban heat island effect.

Overall, these results clearly demonstrate that under heatwave conditions, surface imperviousness, coastal water bodies, and vegetation conditions are the core driving and regulating factors of the urban heat island effect in coastal cities.

The interaction detector results based on the GeoDetector model (**Figure 7**) showed that the interactions among all driving factors exhibit enhancement effects on the spatial heterogeneity of SUHII in the main urban area of Dalian. Most factor pairs demonstrated a bivariate enhancement effect, while only the interaction between NDVI and MNDWI showed nonlinear enhancement, indicating that the urban heat island effect in the study area is driven by multi-factor coupling rather than the independent influence of a single factor.In terms of interaction q values, the strongest explanatory power was observed for the interaction between MNDWI and NDVI (q = 0.86678), followed closely by NDBSI and MNDWI (q = 0.86654), NDBSI and NDVI (q = 0.85983), and NDBSI and POP (q = 0.84756). These results indicate that the synergistic coupling between surface imperviousness and coastal water bodies, vegetation cover, and population concentration constitutes the core mechanism driving the spatial differentiation of the urban heat island pattern. All other factor combinations also show interaction q values

higher than those of individual factors, confirming the widespread amplification effect of multi-factor interactions. Although the interactions involving DEM significantly enhance explanatory power, their overall magnitude remains relatively low, further suggesting that topographic conditions play a limited role in regulating the regional thermal environment.

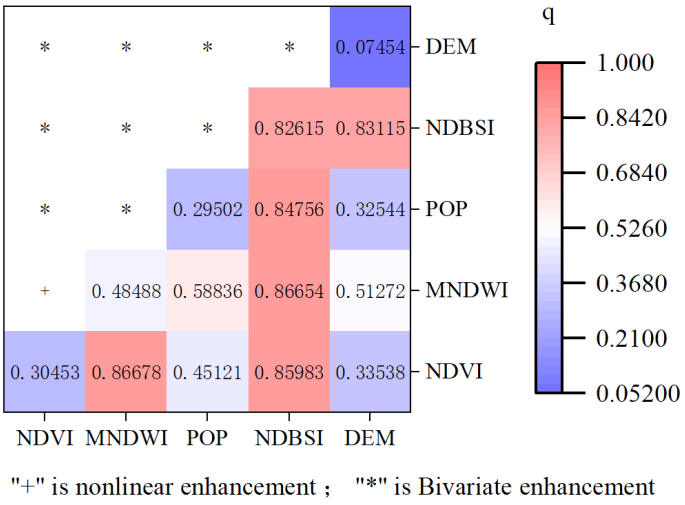

Figure 7. GeoDetector-based interaction analysis of driving factors of the urban heat island effect.

Overall, these findings reveal that under heatwave conditions, surface imperviousness acts as a key driving carrier of the urban heat island effect. Its synergistic interactions with coastal water bodies, vegetation cover, and population concentration jointly shape and amplify thermal environmental risks in coastal cities, providing a refined scientific basis for developing multidimensional and systematic strategies for urban thermal environment optimization and climate adaptation.

4. Conclusions and Perspectives

Based on the Local Climate Zone (LCZ) framework and multi-source environmental factor analysis, this study investigated the characteristics of the urban thermal environment in the main urban area of Dalian under the summer 2018 heatwave conditions. From the perspectives of urban underlying surface structure, thermal environmental response, and driving mechanisms, the formation logic of the urban heat island effect in a coastal cold-region city was systematically revealed. The main conclusions are as follows.

First, the LCZ spatial pattern in the main urban area of Dalian exhibited a pronounced structure characterized by "coastal agglomeration, inland transition, and mountainous ecological mosaics". This reflects the typical spatial morphology of coastal cities constrained by both topography and urban expansion. Built-up areas were dominated by compact and open building types, forming high-density continuous distributions in the urban core and along coastal zones, while natural LCZs were mainly distributed in fragmented patterns within southern mountain-

ous regions and coastal ecological spaces. This structure establishes the fundamental spatial differentiation of the urban thermal environment, where anthropogenic built-up areas dominate heat accumulation, while ecological components act as localized regulatory elements embedded within the urban matrix.

Second, under the combined influence of heatwave conditions, the study area exhibited significantly intensified spatial heterogeneity in its land surface thermal environment. High-temperature zones were strongly coupled with high-density built-up areas and coastal industrial belts, forming continuous agglomerated patterns, whereas low-temperature zones were primarily controlled by water bodies and mountainous vegetation, resulting in a multi-centered and nested cooling source pattern. Overall, the thermal environment demonstrates an unbalanced response characterized by "enhanced warming in built-up areas and localized mitigation in ecological spaces," indicating that coastal cold-region cities also experience substantial amplification of thermal risks under extreme heat events.

Finally, GeoDetector analysis reveals that surface imperviousness is the dominant driver of spatial differentiation in the urban heat island effect, followed by water bodies and vegetation coverage, while population density also plays an important regulatory role. In contrast, topographic factors exert relatively limited influence. Interaction effects among multiple factors predominantly exhibit enhancement effects, with the coupling between surface imperviousness and water bodies, vegetation, and population activity showing the strongest explanatory power for the spatial pattern of SUHII. These findings indicate that urban thermal environment evolution is not driven by a single factor but results from the combined effects of multiple urban components, which further amplify heat island intensity under synergistic interactions.

In summary, from the three dimensions of "underlying surface spatial structure, thermal environmental response patterns, and multi-factor driving mechanisms", this study elucidates the formation pathways and mechanisms of the urban heat island effect in a coastal cold-region city under heatwave conditions. The results demonstrate that even coastal cities traditionally considered cold regions are still subject to significant thermal stress under extreme climate events. These insights provide theoretical support and practical references for urban thermal environment regulation and ecological spatial optimization in similar regions.

Conflicts of Interest

The authors declare no conflicts of interest regarding the publication of this paper.

References

[1] Balchin, W.G.V. and Pye, N. (1947) A Micro-Climatological Investigation of Bath and the Surrounding District. *Quarterly Journal of the Royal Meteorological Society*, **73**, 297-323. https://doi.org/10.1002/qj.49707331706

[2] Wang, S., Zhan, W., Zhou, B., Tong, S., Chakraborty, T., Wang, Z., *et al.* (2025) Dual Impact of Global Urban Overheating on Mortality. *Nature Climate Change*, **15**, 497-504. https://doi.org/10.1038/s41558-025-02303-3

[3] Feng, R., Wang, F., Wang, K., Wang, H. and Li, L. (2021) Urban Ecological Land and Natural-Anthropogenic Environment Interactively Drive Surface Urban Heat Island: An Urban Agglomeration-Level Study in China. *Environment International*, **157**, Article ID: 106857. https://doi.org/10.1016/j.envint.2021.106857

[4] Peng, B.F., Shi, Y.S., Wang, H.F., *et al.* (2013) The Impacting Mechanism and Laws of Function of Urban Heat Islands Effect: A Case Study of Shanghai. *Acta Geographica Sinica*, **68**, 1461-1471. (In Chinese) https://doi.org/10.11821/dlxb201311002

[5] Zhou, W., Cadenasso, M.L., Schwarz, K. and Pickett, S. (2014) Quantifying Spatial Heterogeneity in Urban Landscapes: Integrating Visual Interpretation and Object-Based Classification. *Remote Sensing*, **6**, 3369-3386. https://doi.org/10.3390/rs6043369

[6] Oke, T.R. (1981) Canyon Geometry and the Nocturnal Urban Heat Island: Comparison of Scale Model and Field Observations. *Journal of Climatology*, **1**, 237-254. https://doi.org/10.1002/joc.3370010304

[7] Gong, P., Lan, L., Guo, C. and Guo, R. (2025) A Spatiotemporal Deep Learning Approach to Enhance Air Temperature Estimation Based on the Sole Input of Land Surface Temperature. *Journal of Cleaner Production*, **532**, Article ID: 146887. https://doi.org/10.1016/j.jclepro.2025.146887

[8] Yang, Q., Ye, R., Chakraborty, T., Hu, T. and Liu, Y. (2026) Estimation of Intensity, Footprint, and Capacity of Surface Urban Heat Islands Using a Direction-Enhanced Adaptive Synchronous Extraction (DEASE) Method. *Remote Sensing of Environment*, **333**, Article ID: 115118. https://doi.org/10.1016/j.rse.2025.115118

[9] Jiang, S., Peng, J,. Dong, J., *et al.* (2022) Conceptual Connotation and Quantitative Characterization of Surface Urban Heat Island Effect. *Acta Geographica Sinica*, **77**, 2249-2265. (In Chinese) https://doi.org/10.11821/dlxb202209008

[10] Oke, T.R. (1982) The Energetic Basis of the Urban Heat Island. *Quarterly Journal of the Royal Meteorological Society*, **108**, 1-24. https://doi.org/10.1002/qj.49710845502

[11] Souverijns, N., De Ridder, K., Veldeman, N., Lefebre, F., Kusambiza-Kiingi, F., Memela, W., *et al.* (2022) Urban Heat in Johannesburg and Ekurhuleni, South Africa: A Meter-Scale Assessment and Vulnerability Analysis. *Urban Climate*, **46**, Article ID: 101331. https://doi.org/10.1016/j.uclim.2022.101331

[12] Inostroza, L., Hamstead, Z., Spyra, M. and Qureshi, S. (2019) Beyond Urban-Rural Dichotomies: Measuring Urbanisation Degrees in Central European Landscapes Using the Technomass as an Explicit Indicator. *Ecological Indicators*, **96**, 466-476. https://doi.org/10.1016/j.ecolind.2018.09.028

[13] Stewart, I.D. and Oke, T.R. (2012) Local Climate Zones for Urban Temperature Studies. *Bulletin of the American Meteorological Society*, **93**, 1879-1900. https://doi.org/10.1175/bams-d-11-00019.1

[14] Li, Z., Su, Y., Xia, R. and Pan, Y. (2025) Integrating LCZ Framework and Envi-Met Simulation for Multi-Scale Assessment of Urban Thermal Characteristics and Blue-Green Infrastructure Performance. *Sustainable Cities and Society*, **134**, Article ID: 106969. https://doi.org/10.1016/j.scs.2025.106969

[15] Shi, S., Ji, S. and Luo, Z. (2025) Spatial Heterogeneity, Interaction and Multi-Scale Effects of Driving Factors of Heat Island Intensity in Different Urban Agglomerations. *Sustainable Cities and Society*, **126**, Article ID: 106401. https://doi.org/10.1016/j.scs.2025.106401

[16] Xie, B., Meng, B. and Zhang, M. (2026) Unveiling Vegetation Dynamics and Driving Forces in Karst Regions Using MODIS NDVI and XGBoost-Shap. *Science of Remote Sensing*, **13**, Article ID: 100408. https://doi.org/10.1016/j.srs.2026.100408

[17] Wu, T., Chen, Z., Zhou, S., Huang, R., Xing, P., Li, S., *et al.* (2025) Joint Evaluation of Urban Built Environment's Driving Patterns on Urban Heat Island (UHI) and Urban Moisture Island (UMI). *Sustainable Cities and Society*, **127**, 106450. https://doi.org/10.1016/j.scs.2025.106450

[18] Shen, L., Li, Z., Hao, J., Wang, L., Chen, H., Wang, Y., *et al.* (2025) Evaluating the Dynamic Response of Cultivated Land Expansion and Fallow Urgency in Arid Regions Using Remote Sensing and Multi-Source Data Fusion Methods. *Agriculture*, **15**, Article 839. https://doi.org/10.3390/agriculture15080839

[19] Ferré, J.A., Vernet, A. and Fabregat, A. (2025) Predicting the Impact of the Urban Texture on the Urban Heat Island Intensity Using Machine Learning: The Case for the Iberian Peninsula. *Urban Climate*, **62**, Article ID: 102527. https://doi.org/10.1016/j.uclim.2025.102527

[20] Yang, J., Ren, J., Sun, D., Xiao, X., Xia, J., Jin, C., *et al.* (2021) Understanding Land Surface Temperature Impact Factors Based on Local Climate Zones. *Sustainable Cities and Society*, **69**, Article ID: 102818. https://doi.org/10.1016/j.scs.2021.102818

[21] Li, M., Abuduwaili, J., Liu, W., Feng, S., Saparov, G. and Ma, L. (2024) Application of Geographical Detector and Geographically Weighted Regression for Assessing Landscape Ecological Risk in the Irtysh River Basin, Central Asia. *Ecological Indicators*, **158**, Article ID: 111540. https://doi.org/10.1016/j.ecolind.2023.111540

[22] Feng, Z.X., Wang, S.J., Jin, S.H. and Yang, J. (2019) Effects of Urban Morphology and Wind Conditions on Land Surface Temperature in Changchun. *Acta Geographica Sinica*, **74**, 902-911. (In Chinese) https://doi.org/10.11821/dlxb201905005

[23] Herath, H.M.P.I.K., Halwatura, R.U. and Jayasinghe, G.Y. (2018) Evaluation of Green Infrastructure Effects on Tropical Sri Lankan Urban Context as an Urban Heat Island Adaptation Strategy. *Urban Forestry & Urban Greening*, **29**, 212-222. https://doi.org/10.1016/j.ufug.2017.11.013

[24] Zhao, J., Guo, F., Zhang, H. and Dong, J. (2024) Mechanisms of Non-Stationary Influence of Urban Form on the Diurnal Thermal Environment Based on Machine Learning and MGWR Analysis. *Sustainable Cities and Society*, **101**, Article ID: 105194. https://doi.org/10.1016/j.scs.2024.105194

[25] Stewart Fotheringham, A., Charlton, M. and Brunsdon, C. (1996) The Geography of Parameter Space: An Investigation of Spatial Non-Stationarity. *International Journal of Geographical Information Systems*, **10**, 605-627. https://doi.org/10.1080/02693799608902100

[26] Wei, L. and Sobrino, J.A. (2024) Surface Urban Heat Island Analysis Based on Local Climate Zones Using ECOSTRESS and Landsat Data: A Case Study of Valencia City (Spain). *International Journal of Applied Earth Observation and Geoinformation*, **130**, Article ID: 103875. https://doi.org/10.1016/j.jag.2024.103875

[27] Demuzere, M., Kittner, J., Martilli, A., *et al.* (2022) A Global Map of Local Climate Zones to Support Earth System Modelling and Urban Scale Environmental Science. *Earth System Science Data Discussions*, **14**, 3835-3873. https://doi.org/10.5194/essd-2022-92

[28] Bechtel, B., Demuzere, M., Mills, G., Zhan, W., Sismanidis, P., Small, C., *et al.* (2019) SUHI Analysis Using Local Climate Zones—A Comparison of 50 Cities. *Urban Climate*, **28**, Article ID: 100451. https://doi.org/10.1016/j.uclim.2019.01.005

[29] Lin, Z., Xu, H., Hu, X., Liu, Z., Yao, X. and Zhu, Z. (2024) Characterizing the Seasonal Relationships between Urban Heat Island and Surface Energy Balance Fluxes Considering the Impact of Three-Dimensional Urban Morphology. *Building and Environment*, **265**, Article ID: 112017. https://doi.org/10.1016/j.buildenv.2024.112017